SUPPLEMENTARY ONLINE MATERIAL

Cassini Imaging Science: Initial Results on Saturn's Rings and Small Satellites

C. C. Porco,[1]* E. Baker,[1] J. Barbara,[2] K. Beurle,[3] A. Brahic,[4] J. A. Burns,[5] S. Charnoz,[4] N. Cooper,[3] D. D. Dawson,[6] A. D. Del Genio,[2] T. Denk,[7] L. Dones,[8] U. Dyudina,[9] M. W. Evans,[3] B. Giese,[10] K. Grazier,[11] P. Helfenstein,[5] A. P. Ingersoll,[9] R. A. Jacobson,[11] T. V. Johnson,[11] A. McEwen,[6] C. D. Murray,[3] G. Neukum,[7] W. M. Owen,[11] J. Perry,[6] T. Roatsch,[10] J. Spitale,[1] S. Squyres,[5] P. Thomas,[5] M. Tiscareno,[5] E. Turtle,[6] A. R. Vasavada,[11] J. Veverka,[5] R. Wagner,[10] R. West[11]

[1]Cassini Imaging Central Laboratory for Operations, Space Science Institute, 4750 Walnut Street, Suite 205, Boulder, CO 80301, USA. [2]Goddard Institute for Space Studies, NASA, 2880 Broadway, New York, NY 10025, USA. [3]Astronomy Unit, Queen Mary, London E1 4NS, UK. [4]Centre d'Etudes de Saclay, Université Paris 7, L'Orme des Merisiers, 91191 Gif-sur-Yvette Cedex, France. [5]Department of Astronomy, Cornell University, Space Sciences Building, Ithaca, NY 14853, USA. [6]Department of Planetary Sciences, University of Arizona, 1629 East University Boulevard, Tucson, AZ 85721, USA. [7]Institut für Geologische Wissenschaften, Freie Universität, 12249 Berlin, Germany. [8]Department of Space Studies, Southwest Research Institute, 1050 Walnut Street, Suite 400, Boulder, CO 80302, USA. [9]Division of Geological and Planetary Sciences, California Institute of Technology, 150-21, Pasadena, CA 91125, USA. [10]Institute of Planetary Research, German Aerospace Center, Rutherfordstrasse 2, 12489 Berlin, Germany. [11]Jet Propulsion Laboratory, California Institute of Technology, 4800 Oak Grove Drive, Pasadena, CA 91109, USA.

*To whom correspondence should be addressed. E-mail: carolyn@ciclops.org

Small Satellites

Main-satellite-region searches: Synnott (**S1**) discussed a number of possible satellites in the inner saturnian system, all with diameters $d < 20$ km, assuming albedos similar to those of the known inner moons. Gordon et al. (**S2**, **S3**) reanalyzed Voyager images and found five possible moons in the Mimas-Enceladus region with 2 km $< d <$ 40 km**.** However, all the detections occurred in only a single image and none of the putative moons could be confirmed. A number of possible new satellites were reported during the 1995 Saturn ring-plane crossing (RPX). Two of these objects turned out to be Prometheus and Atlas at unexpected longitudes, and most or all of the others were probably transient clumps within or near the F ring **(47**, **65**, **S4, S5, S6)**. Dones et al. (**S7**) performed a groundbased search during the 1995 ring-plane crossing, and found no moons**.** (**S7**) should have been able to detect moons with $d > 6$ km. Because of scattered light close to the planet, their constraints are strongest exterior to the orbit of Dione (6 Saturn radii).

Ring-region searches: The main imaging sequence designs to detect ring-region satellites are (i) frequent imaging of the ansa of a ring gap or F ring region so that orbiting bodies and ring material can be captured moving through the field of view, and (ii) complete longitudinal scans of specific gaps and narrow rings to search for new ring structures and moons at high resolutions (**1**).

Stability: **Fig. S1** shows the results of integrating the orbits of 1000 test particles in the vicinity of Mimas after 4800 years. The main impactors on the inner satellites of Saturn are thought to be ecliptic comets, bodies on low-inclination heliocentric orbits thought to originate in the Kuiper belt/scattered disk beyond Neptune **(S8).** At an impact speed of 26 km/s, comets only tens of meters in diameter should be able to catastrophically disrupt bodies the size of Methone (S/2004

S1) and Pallene (S/2004 S2). If ecliptic comets have a "collisional'' size distribution, for which the number of cometary nuclei with radii larger than r scales as $r^{-2.5}$, the newly discovered moons would have lifetimes of only ~1 - 10 Myr **(S7, S8)**. While such moons should be able to reaccrete, since they orbit outside of Saturn's Roche limit, this scenario requires that the efficiency of reaccretion be more than 99%. Alternatively, the size distribution of ecliptic comets could be "flatter," *i.e.,* the index of the size-frequency distribution could be considerably smaller than 2.5, as is suggested by crater counts on Europa **(S7, S9)** and possibly by recent Hubble Space Telescope (HST) observations **(S10).** In this case, catastrophic disruption would not occur as frequently.

Orbits: Saturn's satellites Janus, discovered by Dollfus in 1966, and Epimetheus, discovered by Fountain *et al*. in 1977, are known as the "co-orbitals" because they have nearly identical semimajor axes some 15,000 km exterior to the main ring system. Prometheus, Pandora, and Atlas were discovered in imaging data acquired during the Voyager 1 encounter in 1980 (**21**). Prometheus and Pandora lie on either side of Saturn's F ring and are presumed to be radially confining it; Atlas orbits just beyond the outer edge of the A ring. Pan was discovered (**S11**) during an examination of saturnian ring images taken by the Voyager spacecraft; it orbits within the Encke gap.

The satellites Methone (S/2004 S1) and Pallene (S/2004 S2) were discovered in Cassini images taken on 1 June 2004 orbiting between Mimas and Enceladus (**3**). In images from 21 June 2004, S/2004 S3 and S/2004 S4 were discovered orbiting within the F ring (**4**). Initially it was thought that S/2004 S3 and S/2004 S4 might be the same object. However, the only orbit matching both sets of observations crossed the F ring and was considered implausible. Subsequent recovery of

S/2004 S3 on 17 October 2004 has led to an orbit which confirms the uniqueness of the two objects. Using images acquired on 21 October 2004 and 28 October 2004, respectively, Polydeuces (S/2004 S5) was found orbiting near Dione's orbit and S/2004 S6 was found in the region of the F ring (**5**).

The orbits were determined by fitting positional measurements to a set of equinoctial orbital elements. These are: a = geometric semimajor axis; $\lambda = M+\varpi = M+\omega+\Omega$; $h = e \sin \varpi$; $p = \tan(i/2) \sin \Omega$; $k = e \cos \varpi$; and $q = \tan(i/2) \cos \Omega$, where e is the eccentricity, M is the mean anomaly, ω is the argument of periapsis, i is the inclination to Saturn's equator, Ω is the longitude of the ascending node on Saturn's equator, λ is the mean longitude, and ϖ is longitude of periapsis. The longitudes are all measured from the node of Saturn's equator on the equator of the International Celestial Reference Frame. The three longitude rates associated with the elements are $d\lambda/dt$, $d\varpi/dt$ and $d\Omega/dt$.

Initial orbits are generated from the first suite of observations, which are then used to find the new objects in other imaging data by predicting the locations at the times of all the images thus far collected by Cassini. Methone and Pallene were subsequently found in this way in the earlier approach sequences and their orbits were consequently improved by the longer baseline. Such improvements then permitted the acquisition of new Cassini images specifically retargeted to capture the new moons at a future time. Retargeted observations have been collected and used in the orbit fits for Methone, Pallene, and Polydeuces.

Where Voyager measurements have been used, these are the sample and line locations of the satellites seen in Voyager ISS images. Background stars and other satellites in the images provided camera

pointing references for the Atlas observations. The pointing for the Pan observations was determined from the location of the Encke gap and other image features, *e.g.*, the shadow boundary on the rings, Saturn's limb and terminator, and the outer edge of the B ring.

We determined the elements of Atlas from a fit to 5 observations from Voyager 1, 7 from Voyager 2, and 69 from Cassini. The latter were made between 26 May 2004 and 2 June 2004. For Pan we fit 23 Voyager 2 observations and the 23 Cassini observations which were made between 26 May 2004 and 11 October 2004. We fit the orbits of Methone, Pallene, and S/2004 S3 to data from 54, 37, and 20 Cassini images, respectively. Most of the images for Methone and Pallene were taken on 1 June 2004. Additional images for Methone were acquired on 12 May 2004, 2 November 2004, and 3 November 2004. Images taken on 18 April 2004, 25 April 2004, and 3 November 2004 provided additional data for Pallene. Nineteen of the S/2004 S3 images are from 21 June 2004 and one is the recovery on 17 October 2004. There are only 4 observations of S/2004 S4; all occurred on 21 June 2004. The data for S/2004 S5 includes 67 observations beginning on 2 April 2004 and ending on 2 November 2004; and the 17 observations of S/2004 S6 are from 28 October 2004. We summarize parameters of the satellite search sequences in **Table S1**.

Prior to Cassini, the numerically integrated orbits of Janus, Epimetheus, Prometheus, and Pandora had been fit to astrometric observations acquired with HST and from Earth-based observatories and to imaging data acquired from the Voyager spacecraft (**13**). In determining our new orbits for these objects, we incorporated data from more than 4000 Cassini images acquired during the period 6 February 2004 to 19 June 2004. For convenience, however, we did not fit the Voyager data or Earth-based data acquired during the 1966 Saturn ring plane crossing. These data will be added at a later

date. We believe that the extensive set of high quality HST observations together with the recent Earth-based data and the Cassini data are more than sufficient to provide good orbits for the near term.

Rings

Photometry/Color: We averaged the calibrated reflectivity (I/F) of the rings over longitude to compute radial profiles of ring brightness. We then used a multiple-scattering (doubling) code to compute the predicted I/F of the rings for a variety of assumed values of the ring particles' Bond, or overall, albedo. This calculation assumed that the rings' optical depth equals the value measured by the Voyager photopolarimeter experiment (**39**) and that the main rings have the same, highly backscattering, phase function everywhere (**S12**).

The multiple scattering code assumes that the ring particles are well-separated, *i.e.*, that the ring is many particles thick. In reality, in most parts of the main rings, the particles are probably confined to a layer whose thickness is only a few times the size of the largest particles (**S13**). Physically thin rings of moderate-to-high optical depth are typically brighter at low phase angles and darker at high phase angles than physically thick rings, due to reduced amounts of shadowing and multiple scattering, respectively (**S14**, **S15**). At the intermediate phase angle at which our color images were taken, the rings' I/F is less sensitive to the thickness of the particle layer. Therefore, ring particle albedos are better determined in our data than at the small phase angles accessible from the Earth.

The doubling code results were inverted to determine the Bond albedo as a function of radius, which is shown in **fig. S2**. The albedo of the C ring particles generally increases with distance from Saturn at all wavelengths, while the B ring shows complex structure on length scales of hundreds to thousands of

km. The A ring, by contrast, is relatively featureless. The albedo of the particles in parts of the central B ring is ~0.9 in the RED and IR2 filters. Our approach neglects variations in the scattering phase function of different ring regions, which could result from differences in physical thickness or in the surface textures of individual particles. Such variations are likely small enough at the intermediate phase angles of our Cassini observations that most of the albedo variations shown in **fig. S2** represent real differences in ring composition.

Rings at high resolution. To produce profiles of optical depth across the narrow ringlets seen in **figs. 4a** and **4b**, we converted I/F to optical depth (τ), using a doubling code (**fig. S3a** and **S3b**). However, the highest-resolution images taken during SOI viewed the "unlit" face of the rings. In this geometry, I/F does not increase monotonically with τ, as it does for images taken on the "lit" face of the rings. Rather, for small values of τ, I/F increases, but then reaches a maximum at a value of $\tau \sim 0.4$ for the geometry of our images. As τ increases even further, I/F decreases because the layer of particles becomes increasingly opaque. Based upon the Voyager 2 photopolarimeter (PPS) occultation data on the Maxwell and Huygens ringlets, it was clear that the interiors of the ringlets corresponded to the high-optical-depth solution when we converted I/F to τ. However, the exact values of τ we infer depend upon the assumed albedo and scattering model used. Thus, while we believe that the structure shown in **figs. 4a** and **4b** is real, the exact values of optical depth cannot be determined by analysis of images alone.

Waves: Saturn's main rings, particularly the A ring, contain dozens of tightly wound spiral density waves. These waves are excited by Saturn's moons at the sites of gravitational resonances (**42**, **S16**, **S17**, **S18**, **S19**). Mimas also excites several spiral bending waves in the rings (**41**, **S20**, **S21**, **S22**). Both

types of waves show a characteristic decline in wavelength with distance away from resonance which can be used to determine the surface mass density of the rings, σ. The distance over which a wave propagates can be used to estimate the rings' viscosity, and hence physical thickness. Finally, if a wave (or part of a wave) is linear, *i.e.*, the fractional change in surface density, dσ/σ, is much smaller than unity, the mass of the perturbing satellite can be estimated. This technique provided the first estimates for the masses of Prometheus and Pandora, and a crude upper limit on the mass of Atlas (**S19**). The Cassini SOI dark-side images, with their superior resolution and signal-to-noise, contain many waves which were not detected by the instruments on Voyager. For example, we detected several density waves due to the tiny ring moon Atlas, including the 5:4, 9:8, and 10:9 waves (**27**, **40**). We used this technique to model the Atlas 5:4 (**fig. S4a**) and the Pan 7:6 (**fig. S4b**) waves and derive the ring and satellite properties reported in the main text.

To test our fitting procedures, we analyzed the Prometheus 9:8 density wave, a very clean nonlinear wave seen in the Cassini images of the mid-A ring. Our analysis yields a surface density of 39.2 g/cm^2, which lies between the values of 29.0—32.6 g/cm^2 determined by **(S19)**, and the value of 55.0 ± 4.8 g/cm^2 found by (**42**). We infer a viscosity 164 cm^2/s, close to the value of 150 cm^2/s which (**S19**) assumed to fit density waves in the A ring. Using the classical expression for viscosity, this implies a dispersion velocity of 0.3 cm/s and a scale height of 22 meters, considerably larger than we found in the Cassini division, but comparable to values found for the Mimas 5:3 bending wave in the A ring from analysis of Voyager data (**S22**, **S23**). However, since there may be other, "nonlocal" sources of wave damping, our estimate of the scale height in the mid-A ring should be regarded as an upper limit (**49**, **50**).

We also attempted to estimate the mass of Prometheus from the amplitude of the 9:8 wave. However, our conversion from I/F to τ gave a surprisingly large background optical depth (0.85) and small Bond albedo (0.30) in the wave region. Our fit value for Prometheus' GM is 0.007 km^3/s^2, which is about one-half the value found by (**13**) and (**48**). We suspect the discrepancy is due to inadequate modeling of the nonlinear wave, as the values of (**13**) and (**48**) were determined by modeling the direct interactions between Prometheus and Pandora.

Pan wakes: **Figure S5** shows a scan across the image shown in **fig. 5g**, and the result of a wavelet analysis of the scan. Power due to *both* first- and second-order wakes created by Pan is present.

F ring region: A sequence of NAC images of Saturn's right ansa, taken over 16 hours on 20–21 June 2004 as part of a search for small satellites, yielded 83 useful images of the F ring region at a radial resolution as fine as 20 km per pixel. This was the last sequence to provide complete azimuthal coverage of the F ring before SOI. The images were analyzed by re-projecting the region in the radial range from 138,000 km to 142,000 km and a longitude range from 167˚ to 187˚ into a longitude-radius system.

Figures 6 and 7 of (**61**) show how the mechanism that produces gaps and streamers works for two individual particles. Their observed behavior is entirely consistent with that seen in (**60**) and the dominant role of tangential forces in changing semi-major axes. It is likely that the resolution in **fig. 8a** was insufficient to detect a gap, although the discontinuity and streamer are visible.

Poulet *et al.* (**65**) and Barbara and Esposito (**6**) both predict the presence of a belt of ~1 km moonlets in the F ring in order to explain the features detected during the 1995/6 ring plane crossings; such moonlets could even be loosely bound "rubble piles," the disruption of which could give rise to "burst" events (**S24**).

A satellite embedded in the F ring core could produce strands by creating a chaotic zone between 1.5 and 3 Hill radii on either side of its orbit (**S25**, **S26**) while maintaining material co-orbital with itself. However, for the F ring this would imply a satellite with a radius ~60% that of Prometheus, *i.e.*, a radius of ~30 km, and we consider this to be unlikely.

New rings comparable to the jovian ring have been seen in between the outer edge of the A ring and the F ring. One is coincident with Atlas' orbit. **Figure S6** shows radial brightness profiles taken through this region, using different fits for the scattered light background, from which optical depths have been derived under different particle size distribution assumptions (see Table 3 in the main text).

References

S1: S. P. Synnott, *Icarus* **67**, 189 (1986)
S2: M. K**.** Gordon, C. D. Murray, K. Beurle, S. P. Synnott, *IAU Circular* **6162**, 1 (1995)
S3: M. K**.** Gordon, C. D. Murray, K. Beurle, *Icarus* **121**, 114 (1996)
S4: A. S. Bosh, A. S. Rivkin, *Science* **272**, 518 (1996)
S5: P. D. Nicholson, et al., *Science* **272**, 509 (1996)
S6: S. Charnoz, A. Brahic, C. Ferrari, I. Grenier, F. Roddier, P. Thébault, *Astron. Astrophys.* **365**, 214 (2001)
S7: L. Dones, et al., *Icarus*, in press
S8: K. Zahnle, P. Schenk, H. Levison, L. Dones, *Icarus* **163**, 263 (2003)
S9: E. B. Bierhaus, C. R. Chapman, W. J. Merline, *Nature*, in press
S10: G. M. Bernstein, D. E. Trilling, R. L. Allen, M. E. Brown, M. Holman, R. Malhotra, *Astron. J.* **128**, 1364 (2004)
S11: M. R. Showalter, *Nature* **351**, 709 (1991)
S12: L. Dones, J. N. Cuzzi, M. R. Showalter, *Icarus* **105**, 184 (1993)
S13: J. N. Cuzzi, R. H. Durisen, J. A. Burns, P. Hamill, *Icarus* **38**, 54 (1979)
S14: C. C. Porco, H. B. Throop, D. C. Richardson, *Bull. Amer. Astron. Soc.* **33**, 1091 (2001)
S15: H. Salo, R. Karjalainen, *Icarus* **164**, 428 (2003)
S16: J. N. Cuzzi, J. J. Lissauer, F. H. Shu, *Nature* **292**, 703 (1981)
S17: J. B. Holberg, *Astron. J.* **87**, 1416 (1982)
S18: L. W. Esposito, C. C. Harris, K. E. Simmons, *Astrophys. J. Supp. Series* **63**, 749 (1987)
S19: P. A. Rosen, G. L. Tyler, E. A. Marouf, J. J. Lissauer, *Icarus* **93**, 25 (1991)
S20: F. H. Shu, J. N. Cuzzi, J. J. Lissauer, *Icarus* **53**, 185 (1983)
S21: J. J. Lissauer, *Icarus* **62**, 433 (1985)
S22: D. L. Gresh, P. A. Rosen, G. L. Tyler, J. J. Lissauer, *Icarus* **68**, 481 (1986)
S23: J. J. Lissauer, F. H. Shu, J. N. Cuzzi, in Proceedings of IAU Colloquium 75, *Planetary Rings*, ed. A. Brahic, p. 385 (1984)
S24: M. R. Showalter, *Science* **282**, 1099 (1998)
S25: J.-M. Petit, M. Hénon, *Icarus* **66**, 536 (1986)
S26: J. Hänninen, *Icarus* **103**, 104 (1993)
S27: C. Torrence, G. P. Compo, *Bull. Amer. Meteorological Soc.* **79**, 61 (1998)

TABLES

Table S1: Description of satellite search sequences

Observation Name	#Images	Exp (sec)	Start Date	End Date	Region (10^3) (km)	Distance(10^6) (km)
C42OT_APPSATSRC	52	82.0	Feb. 9, 2004	Feb. 16, 2004	500 to 2,000	64.90
C43OT_APPSATSRC	121	82.0	Feb. 23, 2004	Mar. 29, 2004	300 to 1,800	51.29
C44OT_APPSATSRC	288	18.0	Apr. 2, 2004	May 12, 2004	180 to 650	35.23
000RI_SATSRCHBP	322	1.2/4.6	May 26, 2004	June 1, 2004	80 to 250	16.98
00ARI_RNGHAZARD	94	1.0/5.6	Oct. 21, 2004	Oct 22. 2004	166 to 355	3.1

FIGURES

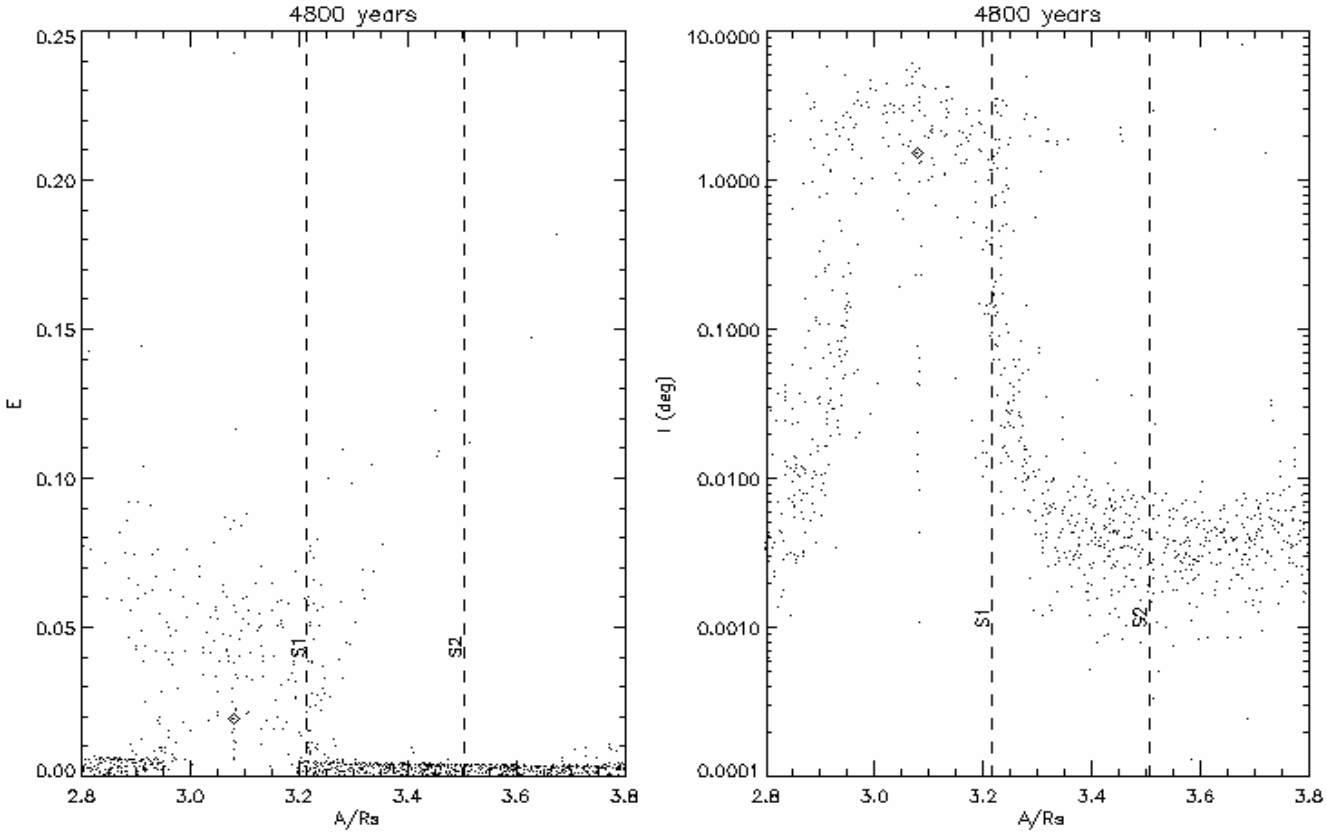

Figure S1: Eccentricity and inclination versus semi-major axis of 1000 test particles in the neighborhood of Mimas (which is shown as a diamond in each panel) after 4800 years of integration (including the influence of Saturn's major satellites and also its J_2 and J_4 gravitational moments). The dashed lines show the semi-major axes of satellites Methone (S/2004 S1) and Pallene (S/2004 S2). Note that this simulation, unlike that of previous workers (**10**), does not incorporate collisions with Mimas; however, as in previous work (**10**), particles within ± 0.09 R_s of Mimas's semi-major axis, where R_s equals Saturn's equatorial radius, are cleared out with a half-life of only ~100 years.

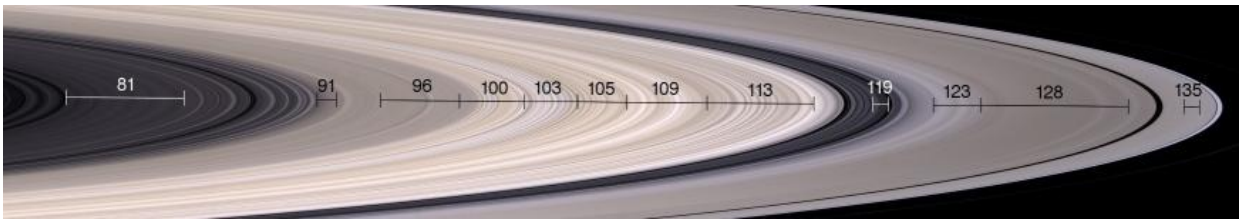

Figure S2a: A natural-color mosaic of Saturn's main rings, indicating the regions whose spectra are shown in **fig. 3**. The average distance from Saturn's center in units of 1000 km is indicated for each region.

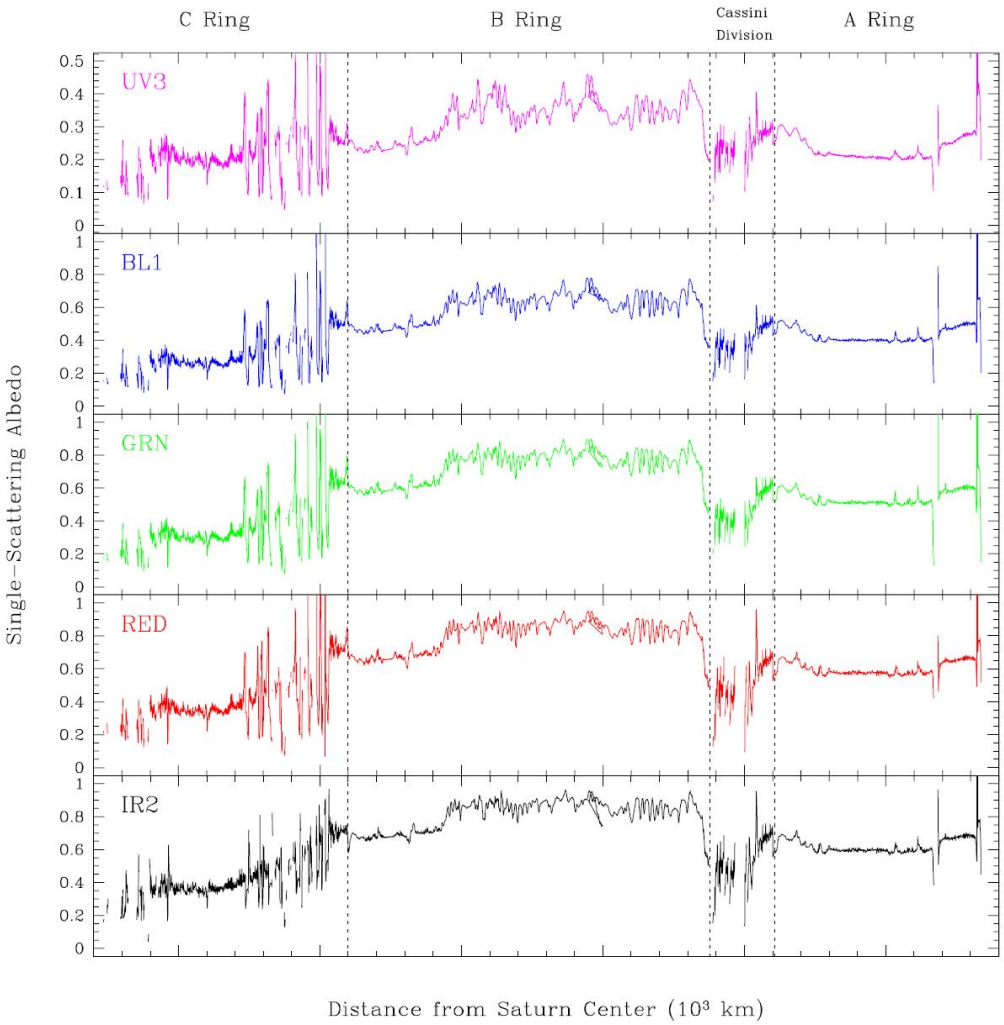

Figure S2b: Inferred Bond albedo of the particles in Saturn's main rings as a function of wavelength. From top to bottom, the panels show albedos inferred for the UV3 (338 nm), BL1 (451 nm), GRN (568 nm), RED (650 nm), and IR2 (862 nm) filters. The vertical scale is the same in each panel except for the UV3 filter. Most of the fine-scale structure in the B ring is real, while most narrow features in the outer C ring, Cassini division, and A ring result from imperfect alignment of gaps in these images.

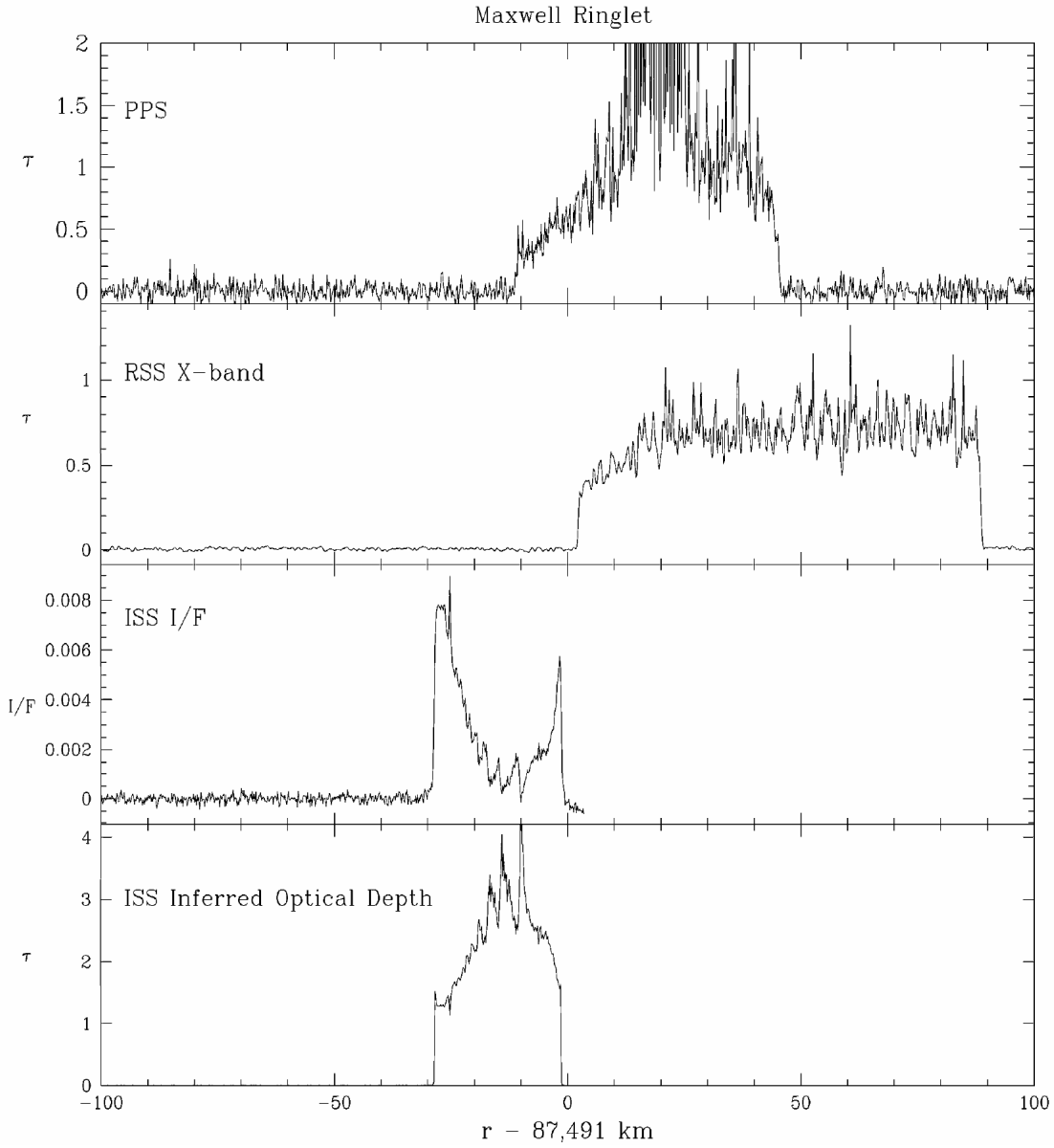

Figure S3a: Structure of the Maxwell ringlet in Saturn's C ring. The top panel shows the optical depth profile of the ringlet in Voyager photopolarimeter (PPS) occultation data; parts of the ringlet have optical depth > 2 and are saturated in this plot because very few stellar photons penetrated the ring. The second panel shows the ringlet's profile in Voyager radio science (RSS) data. Both the average distance of the ring from Saturn and its width are different in the PPS and RSS data, indicating that the ring is eccentric. The third panel shows a longitudinally averaged radial I/F scan through the Maxwell ringlet seen in **fig. 4a**. The bottom panel gives a plausible reconstruction of the ringlet's profile of optical depth vs. distance from Saturn from the radial I/F scan. For images taken in diffuse transmission, there are two solutions for τ for a given value of I/F, so our solution for τ is non-unique.

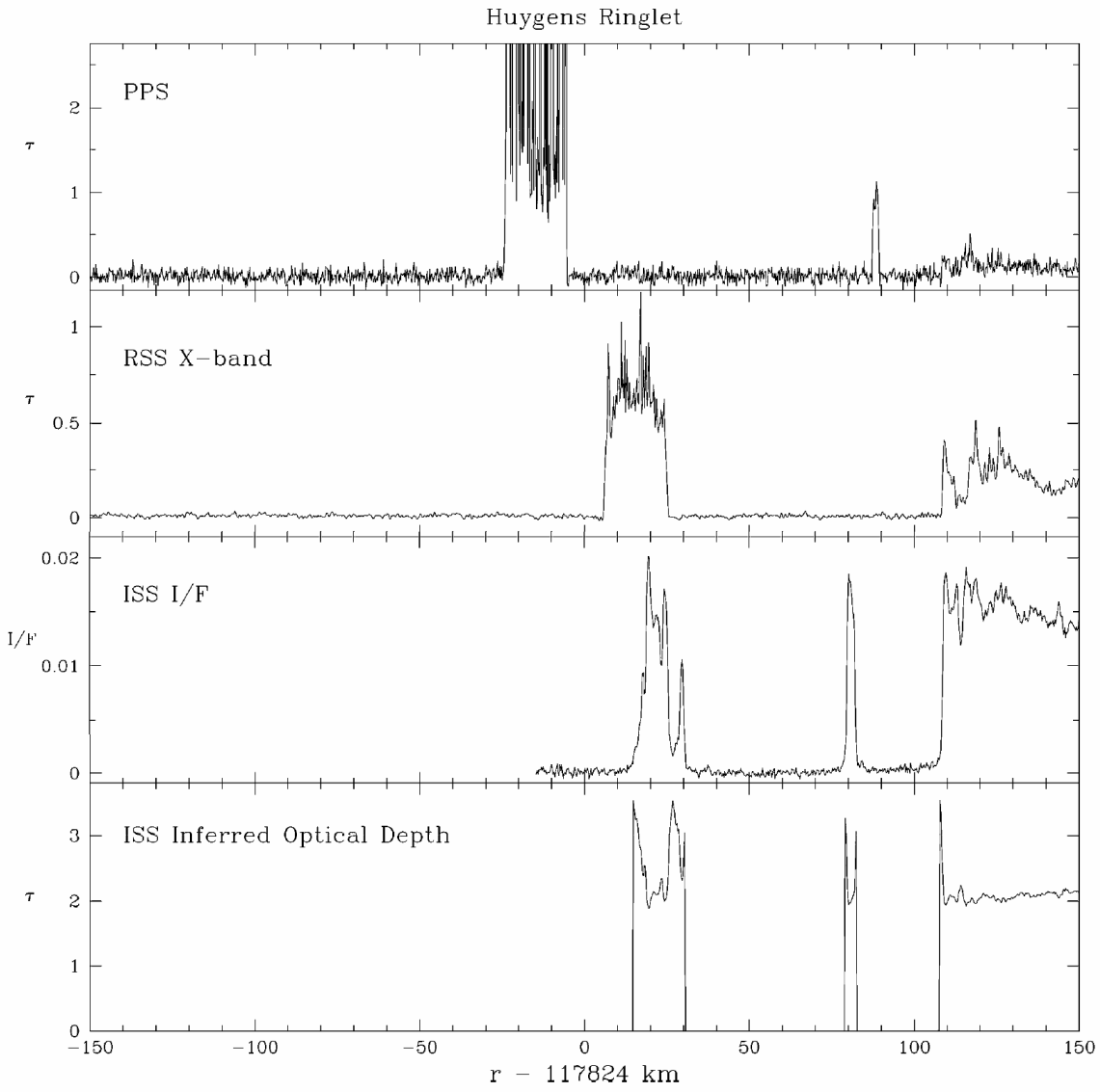

Figure S3b: Structure of the innermost Cassini division, including the narrow Huygens ringlet seen on the left in **fig. 4b**. The four panels in this figure are in the same format as in **fig. S3a**. The Huygens ringlet is the leftmost feature in the four panels, and is about 20 km wide at the longitude of our SOI observations. The optical depths of the narrow ringlet and plateau exterior to the Huygens ringlet are not well-constrained; the plateau, in particular, could have $\tau \sim 0.1$.

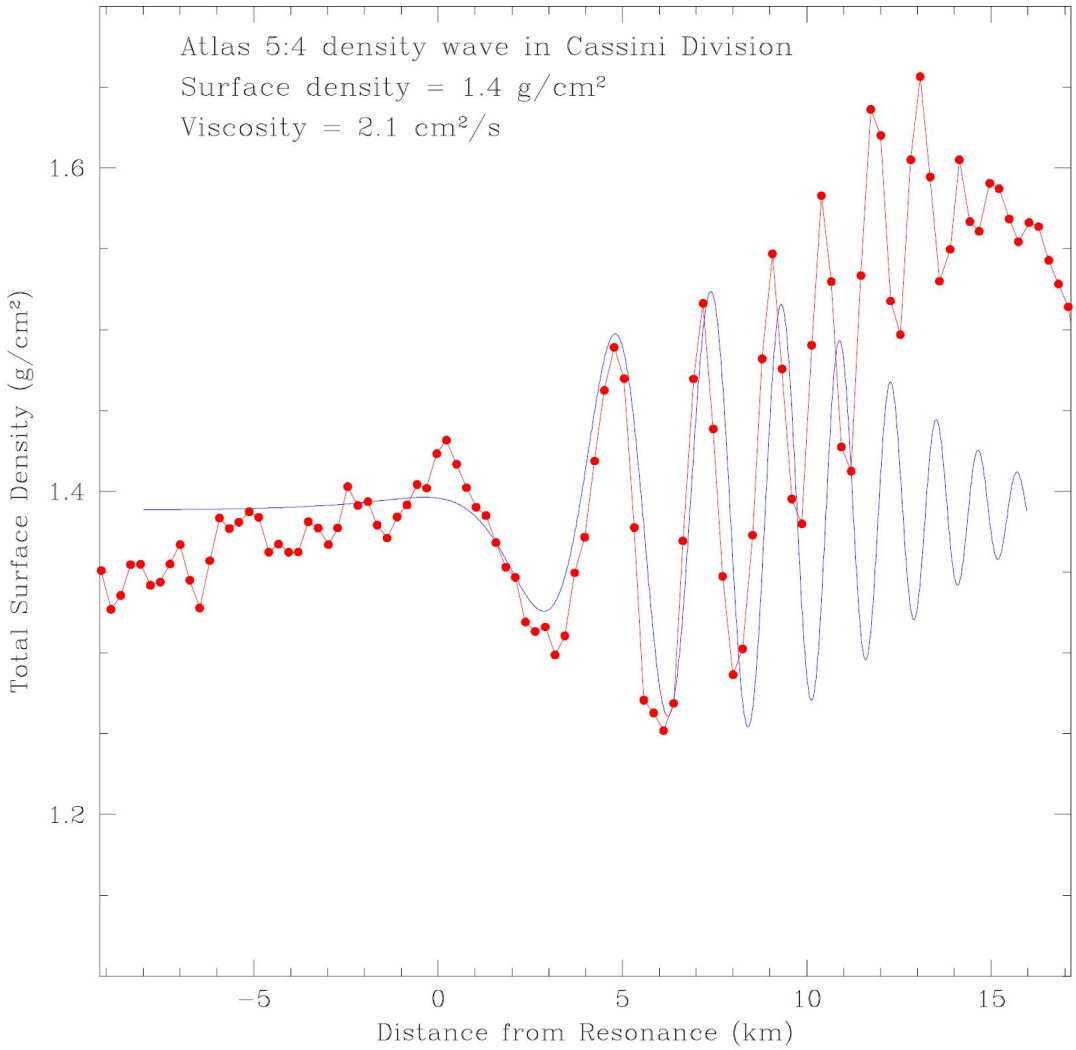

Figure S4a: Observed and model profiles for the Atlas 5:4 density wave in the inner Cassini division. We first fit the wavelength as a function of distance from resonance in the measured I/F profile to determine the surface density of the rings and the location of the Atlas 5:4 inner Lindblad resonance. We then converted the I/F profile to an optical depth profile by assuming the ring particles have a Bond albedo of 0.3 and a backscattering phase function like that of the galilean satellite Callisto. (In this region, the results are not sensitive to the assumed ring scattering properties, because the ring has a sufficiently low optical depth that the light transmitted through the ring is dominated by singly-scattered photons.) Next, we assumed that the surface density is linearly proportional to the optical depth within the wave region (*i.e.*, the particle size distribution remains constant). Finally, we constructed a series of theoretical linear wave profiles in which we varied Atlas' mass, M_{Atlas}, and the damping length, L, which is related to the viscosity. We determined the best fit values of M_{Atlas} and L by using a Levenberg-Marquardt non-linear least squares algorithm. The theoretical profile fits the observed wave well for the first several cycles, but the observed profile shows a "ramp" in background brightness some 10 km external to the resonance. This cause of this ramp is unknown, but could result from changes in the particle size distribution of the rings.

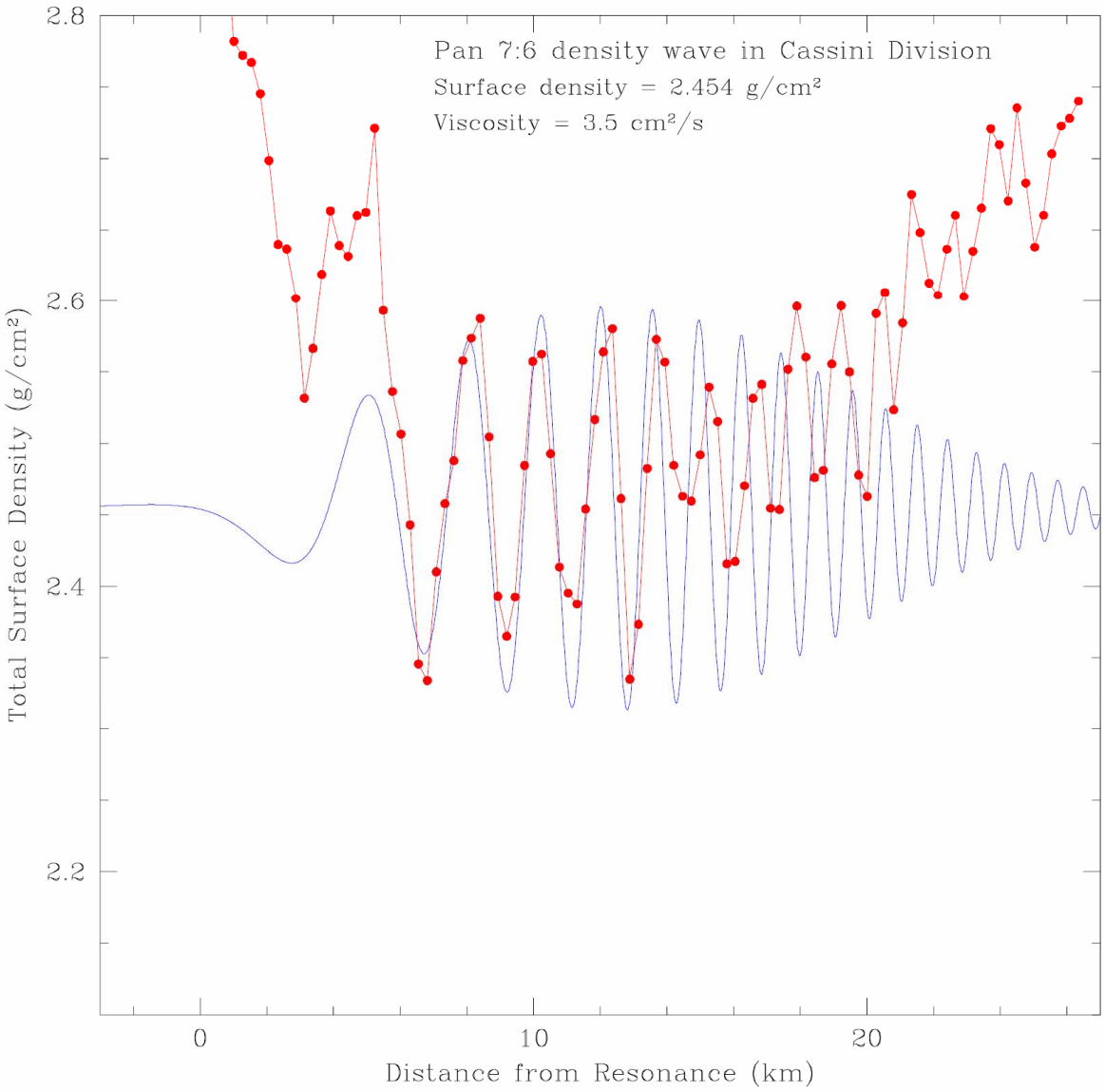

Figure S4b: Observed and model profiles for the Pan 7:6 density wave in the outer Cassini division. We followed procedures similar to those in **fig. S4a**. Here we assumed a Bond albedo of 0.25. The observed profile shows different background brightnesses both interior and exterior to the wave region. The "observed" profile is less certain than the profile shown in **fig. S4a** because the higher optical depth here makes the conversion from I/F to τ and surface density more highly model-dependent.

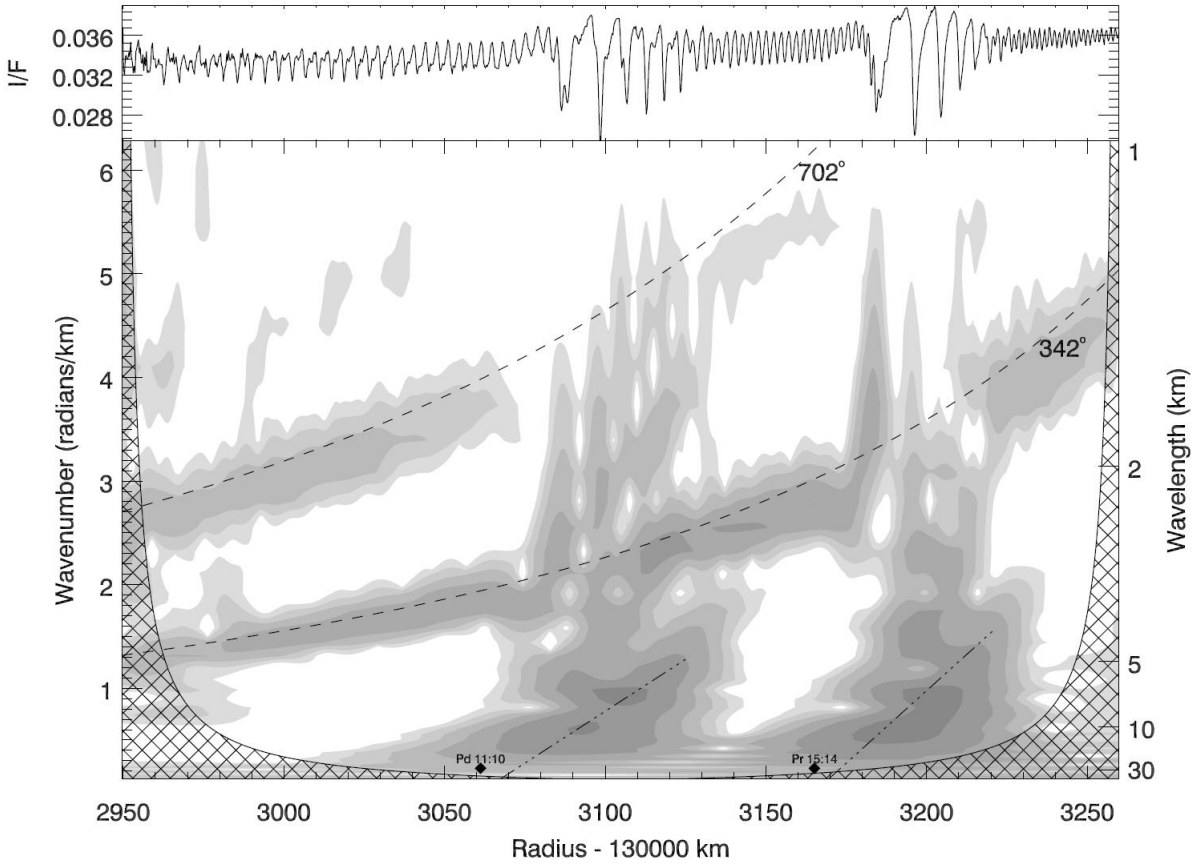

Figure S5: (upper) A radial scan of the brightness (I/F) vs. distance from Saturn's center in image N1467346329 (**fig. 5g**). (lower) A wavelet analysis [**S27**] shows the power contained in the frequency spectrum as a function of radius. The scale is logarithmic, with two shading contours per order of magnitude in the power. The dashed lines give the wake features expected to be caused by Pan at post-encounter longitudes of 342˚ ("first-order") and 702˚ ("second-order"). The dot-dashed lines show the predicted locations of spiral density waves for the Pandora 11:10 and Prometheus 15:14 resonances. In the cross-hatched region (the "cone of influence"), the signal is contaminated by edge effects.

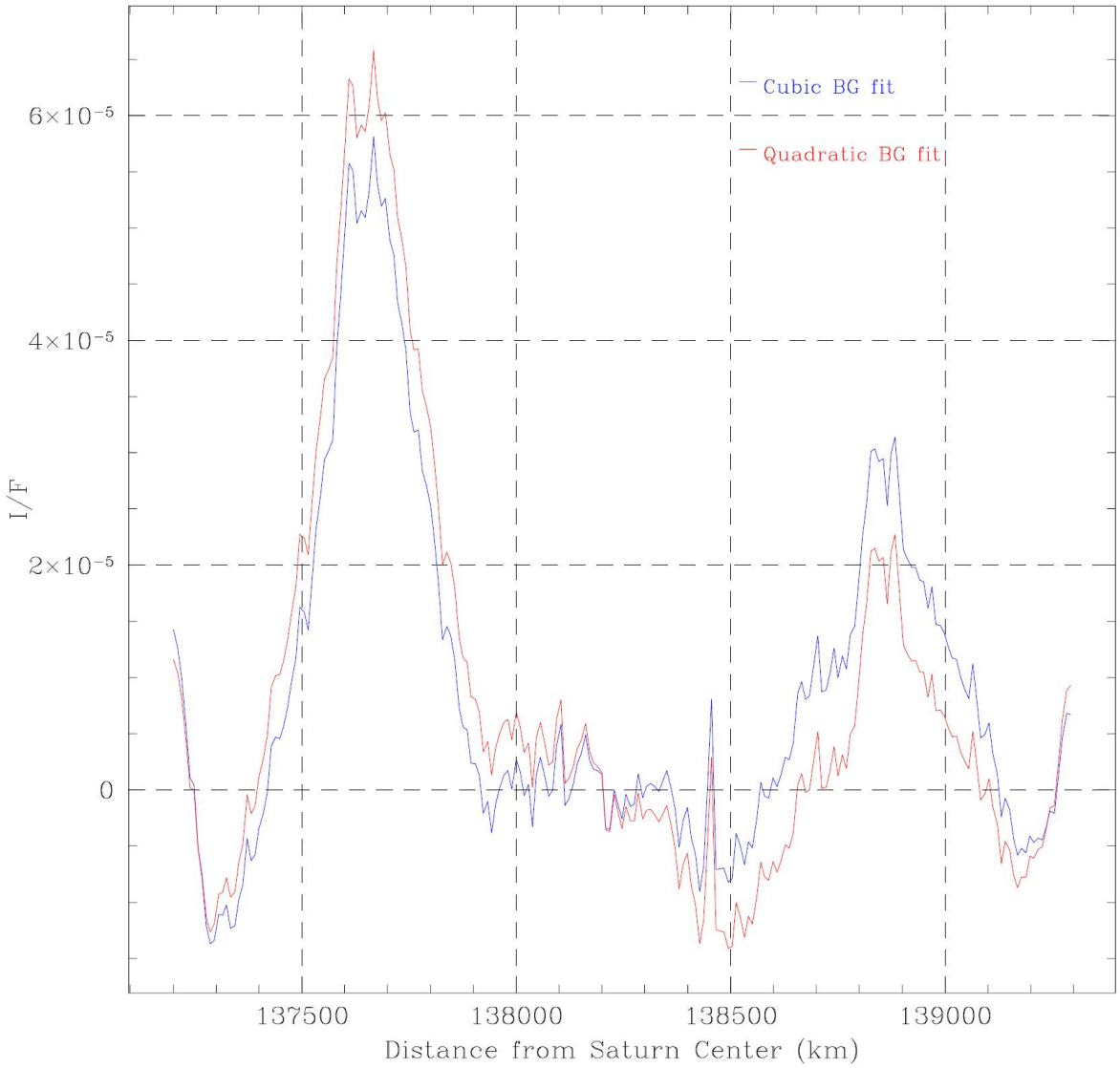

Figure S6: Radial brightness profile of two newly discovered faint rings: R/2004 S1, which is co-located with Atlas' orbit at 137,630 km from the center of Saturn, and R/2004 S2, which is centered at 138,900 km, near the periapse distance of Prometheus' orbit. The image used to construct this profile contains a large amount of scattered light. The profile was constructed by assuming that the regions between the A ring and Atlas' orbit, and between R/2004 S1 and R/2004 S2, are devoid of ring material. With this assumption, second- and third-order fits to the scattered light as a function of distance from Saturn were calculated, and the scattered light fit was subtracted from the raw image profile. The maximum I/F values of R/2004 S1 and R/2004 S2 are approximately 6 x 10^{-5} and 3 x 10-5, respectively, indicating that these rings have optical depths $\tau << 1$ (Table 3 in main text).